# Self-Assembled Diblock Copolymer "Nanoreactors" as "Catalysts" for Metal Nanoparticle Synthesis

**Oz Gazit,[†] Rafail Khalfin,[†] Yachin Cohen,[†] and Rina Tannenbaum*[,†,‡]**

*Department of Chemical Engineering, Technion − Israel Institute of Technology, Haifa, Israel, and School of Materials Science and Engineering, Georgia Institute of Technology, Atlanta, Georgia 30332*

*Received: August 28, 2008; Revised Manuscript Received: November 03, 2008*

The self-assembly and selective distribution of metal or metal oxide nanoparticles in block copolymer matrices was designed to produce photonic bandgap materials through a bottom-up method rather than the more common top-down approach. The synthesis of such materials consists of the in situ thermolysis of metal carbonyl precursors in a diblock copolymer solution. Reaction rates of the formation of nanoparticles in solution were measured to better understand and control the course and final products of the reactions. Our results showed that the rates for reactions performed in a diblock copolymer solution are much faster than the rates of the same reactions performed in a homopolymer solution. The reaction rates for the thermolysis of three different metal carbonyl precursors, $Cr(CO)_6$, $Fe(CO)_5$, and $Co_2(CO)_8$, show that this phenomenon is not specific to the type of metal carbonyl precursor, but rather, to the type of polymer in solution. Polystyrene (PS) and poly(methyl methacrylate) (PMMA) were used as a model system both as homopolymers and as diblock copolymers. Our results showed that the arrangement of the diblock copolymers in solution into spherical internal−external (i.e., core−shell) domains created self-assembled "nanoreactors" with PS acting as the surrounding shell while the internal PMMA domain (core) contained high precursor concentration, resulting in faster kinetics. Furthermore, we have found that the arrangement of the diblock copolymer into these ordered structures in solution does not occur spontaneously, but is rather facilitated by a synergistic coupling effect with the metal carbonyl precursor.

## 1. Introduction

The formation of photonic band gap (PBG) materials having the required periodic dielectric characteristics[1] can be achieved through the use of a top-down approach, that is, fabrication methods that include lithography, layering, and etching processes.[2−4] Conversely, the bottom-up approach can be implemented in this case by using materials that can self-assemble into well-defined periodic structures. The main advantage of this latter approach is the ability to set the properties of the material at the basic molecular level such that they will translate through all length scales and will allow a hierarchical organization of the material into the final structure with the desired periodicity.[5] An important example of such self-organizing materials is block copolymers (BCP), consisting of chemically different segments in a single polymer chain that phase separate due to unfavorable free energy of mixing and form a variety of structures having one-, two-, or three-dimensional ordering.[6−8] By controlling the chemical makeup of the blocks, their length and architecture, it is possible to generate a variety of periodic structures.[5−14] The relationship between the block domain size, its refractive index, and the resulting optical applicability of the BCP is given by the expression $\bar{d}_i \approx \lambda/4n_i$ (where $n_i$ is the refractive index and $\bar{d}_i$ is the optical width, that is, block domain size of the $i$th domain, which is directly related to the molecular weight of the block). However, the molecular weight of a block (i.e., domain spacing) in a BCP that could produce a bandgap in the visible (∼600 nm) or near-IR (∼1000 nm) range would need to be upward of 500 kg/mol (assuming a typical refractive index of a polymer of ∼1.5).[1] By adding nanoscale scatterers, such as metallic nanoparticles (NPs), to the BCP without damaging its spatial alignment, it would be possible to increase its refractive index even at relatively low molecular weights.[15] Upon transmission of light through such a nanocomposite, scattering intensity is substantially reduced when particle dimension is below 50−100 nm, and the optical characteristics of the composite material were shown to be strongly dependent on the particle size, shape, and the interactions between the polymer matrix and the metallic nanoclusters.

Using a di-BCP composed of two segments with different affinities toward particular metallic nanoparticles provides the ability to direct NPs such that they will reside in one domain and not the other, and hence the spatial distribution of the NPs will conform to the BCP morphology.[5,16,17] The selective incorporation of metallic NPs into one of the BCP domains would substantially increase that domain's refractive index. This would enable the use of smaller domains obtained by lower molecular weight BCPs, which would provide better control over the processibility characteristics of the BCP composite film.[18]

Most techniques used to date for the incorporation of NPs into selective BCP domains are complex and require mediating molecules between the BCP and the NPs.[10,19,20] Conversely, the thermolysis of organometallic precursors conducted directly in the BCP solution facilitates the formation of NPs with controlled size and distribution according to the specific chemical reactivity of the polymer blocks. This allows, in turn, the direct self-assembly of the periodic BCP microstructures already containing

* Corresponding author. E-mail: rinatan@technion.ac.il, rinatan@mse.gatech.edu.
† Technion − Israel Institute of Technology.
‡ Georgia Institute of Technology.

10.1021/jp807668h CCC: $40.75 
Published on Web 12/16/2008

the NPs.[12,21−23] In this work, we concentrated on this latter approach, that is, the in situ synthesis of NPs in the BCP solution and the subsequent self-assembly of the NP-containing polymer composites into periodic structure dictated by the thermodynamic equilibrium of the specific BCP system. The BCP segments were chosen such that one domain would have a stronger affinity toward the metallic nanoparticles than the other. In this work, polystyrene-*b*-poly(methyl-methacrylate) diblock copolymer (PS-PMMA) was chosen as a model system. In this system, we expect the NPs to concentrate solely in the PMMA domain, based exclusively on the expected polymer−metal interactions of both blocks with various transition metals or transition metal oxides, without the need to coat the surface of the NPs to render them compatible with a given polymer block.

The thermodynamic behavior of BCPs in dilute solutions has been the subject of extensive experimental and theoretical research (few are mentioned here).[24−27] The structure and conformation of the polymer during the thermolysis reaction of the organometallic precursor may play a critical role in the self-assembly of the metal NPs and on the adsorption of the polymeric chains on the surface of the NP, a process that is responsible for their incorporation into the domain of the more reactive polymer block.

Although polymer adsorption on the NP surfaces was extensively studied both by our group and by others, no correlation was made to date between the characteristics of this process and the thermodynamically driven arrangement of the polymer chains in solution, that is, the possibility of the formation of micelle, globules, and/or free coils.[5,21,22,28−30] We have previously shown that the kinetic characteristics of the formation of NPs in a polymeric medium may shed light on the intimate interactions between the nucleating metallic fragments and the polymer chains in their immediate vicinity, and give an indication as to the mechanism of nucleation and growth of the nanoparticles in that particular environment.[22,31] BCPs represent a particularly interesting system because the chemical differences between the two blocks have the potential to influence, in different ways, the nucleation and growth of the NPs in each block. Moreover, the incompatibility in the chemical makeup between the two BCP segments is expected to lead to a microphase separation of the metal/BCP composite film, creating a periodic composite material that could possess the characteristics of a desired PBG material.

In this work, we examined the formation of chromium, iron, and cobalt oxide NPs ($Cr_2O_3$, $Fe_2O_3$, and $Co_2O_3$) by the decomposition of their corresponding metal carbonyl precursors in homopolymer and BCP solutions. The polymers used were polystyrene (PS), poly(methyl methacrylate) (PMMA), and poly(styrene-*b*-methyl methacrylate) (PS-*b*-PMMA). Comparison between the kinetic and mechanistic features of the organometallic precursor decomposition for all metals revealed a strong and general correlation with the type of polymer in the solution. This work is concerned with the origin, nature, and potential application of this kinetic behavior.

## 2. Experimental Methods

**2.1. Kinetics of the Decomposition Reactions.** Kinetic data were collected using a Thermo-Nicolet 8700 Fourier transform infrared spectrophotometer (FTIR) in a liquid cell equipped with KBr lenses.

***2.1.1. Formation of Chromium Oxide from $Cr(CO)_6$.*** A polymer such as PS ($\bar{M}_n$ = 44 100 g/mol, PDI = 1.03, Polymer Source), PMMA ($\bar{M}_n$ = 46 500 g/mol, PDI = 1.04, Polymer Source), or PS-*b*-PMMA ($\bar{M}_n$ = 21 000-*b*-21 000 g/mol, PDI = 1.07, Polymer Source) was dissolved in cyclohexanone ($C_6H_{10}O$, 99.5%, $d$ = 0.947 g/cm$^3$, bp = 155 °C, Fluka) to form a 2 wt % polymer solution. A second solution of chromium hexacarbonyl (0.01 M) (99% $Cr(CO)_6$, $d$ = 1.77 g/cm$^3$, Aldrich) in cyclohexanone was also prepared. Reaction began with the mixing of both solutions in a 1:1 ratio in a flask held at a constant temperature of 90 °C under a constant nitrogen purge. During the reaction, aliquots were extracted from the flask and quenched with an equal volume of cold solvent. The rate of $Cr(CO)_6$ precursor decomposition was determined by monitoring the variations in the intensity of the strong absorption bands at 1977 cm$^{-1}$, corresponding to the symmetric stretching vibrations of the carbonyl groups.

***2.1.2. Formation of Cobalt Oxide from $Co_2(CO)_8$.*** A polymer PS ($\bar{M}_n$ = 100 000 g/mol, PDI = 1.04, Polyscience, Inc.), PMMA ($\bar{M}_n$ = 110 000 g/mol, PDI = 1.17, Polyscience, Inc.), or PS-*b*-PMMA ($\bar{M}_n$ = 25 300-*b*-25 900 g/mol, PDI = 1.06, Polymer Source) was dissolved in toluene ($C_7H_8$, 99.5+%, $d$ = 0.865 g/cm$^3$, bp = 110 °C, Sigma-Aldrich) to form a 2 wt % solution. A second solution consisting of 0.01 M of dicobalt octacarbonyl (99% $Co_2(CO)_8$, <5% hexane stabilizer, Acros) in toluene was also prepared. Reaction began with the mixing of both solutions in a 1:1 ratio. During the reaction, aliquots were extracted from the flask and quenched with an equal volume of cold solvent. The rate of $Co_2(CO)_8$ precursor decomposition was determined by monitoring the variations in the intensity of the strong absorption bands at either 2019 cm$^{-1}$, corresponding to the symmetric stretching vibrations of the carbonyl groups, or 1866 cm$^{-1}$, corresponding to the stretching vibrations of the bridging carbonyls of one of the $Co_2(CO)_8$ isomers (having a concentration that is directly proportional to the total $Co_2(CO)_8$ isomer concentration). The decrease in the intensity of the two bands (despite the fact that their molecular extinction coefficient is different) gave the same kinetic profile.

***2.1.3. Formation of Iron Oxide from $Fe(CO)_5$.*** A polymer PS ($\bar{M}_n$ = 100 000 g/mol, PDI = 1.04, Polyscience, Inc.), PMMA ($\bar{M}_n$ = 110 000 g/mol, PDI = 1.17, Polyscience, Inc.), or PS-*b*-PMMA ($\bar{M}_n$ = 21 000-*b*-21 000 g/mol, PDI = 1.07, Polymer Source) was dissolved in toluene ($C_7H_8$, 99.5+%, $d$ = 0.865 g/cm$^3$, bp = 110 °C, Sigma-Aldrich) to form a 2 wt % solution. A second solution consisting of 0.01 M of iron pentacarbonyl (99% $Fe(CO)_5$, $d$ = 1.59 g/cm$^3$, Aldrich) in toluene was also prepared. Reaction began upon the mixing of both solutions in a 1:1 ratio in a flask held at a constant temperature of 90 °C under a constant nitrogen purge. During the reaction, aliquots were extracted from the flask and quenched with an equal volume of cold solvent. The rate of $Fe(CO)_5$ precursor decomposition was determined by monitoring the variations in the intensity of the strong absorption bands at 1996 cm$^{-1}$, corresponding to the symmetric stretching vibrations of the carbonyl groups.

**2.2. Particle and Polymer Morphology in Solution Characterization.** Particle size and morphology were examined by transmission electron microscopy (TEM) using both a Philips CM-120 and a FEI Tecnai G2T12 instrument. Images were recorded digitally by a Gatan MultiScan 791 cooled-CCD and a US1000 camera system, respectively. The operating voltage was 120 keV for both microscopes. Samples were prepared by placing a drop of the reaction output on a carbon-coated copper grid (Ted Pella, Inc.), and the excess solvent was blotted off.

Vitrified specimens for cryo-TEM were prepared in a Controlled Environment Vitrification System (CEVS), where temperature and relative humidity are controlled. A drop of about 3 $\mu$L was placed on a copper grid covered with a

perforated carbon film, which in turn was held by tweezers attached to a spring-loaded plunging device. Most of the liquid was blotted away, leaving behind thin (ideally 100−200 nm thick) liquid films supported on the edges of the 3−10 $\mu$m holes. Upon activation of the plunging mechanism, the grid was propelled through an opening trap door into a reservoir of liquid nitrogen at its freezing point, and thus the liquid was vitrified. The specimens were stored under liquid nitrogen and examined at −174 °C by holding them in a Gatan cooling holder. The specimens were imaged at minimal electron dose conditions to minimize beam damage. Images were recorded digitally by a US1000 cooled-CCD camera system.

Small-angle X-ray scattering (SAXS) experiments were performed using a small-angle diffractometer (JJ X-Ray System) including a sealed tube generator with microfocus graded mirror optics providing Cu $K_\alpha$ radiation (Osmic MicroMax), three-pinhole collimation (that results in a beam of 100 $\mu$m in diameter), and a 20 × 20 cm$^2$ two-dimensional position-sensitive wire detector (1024 × 1024 pixels) that was positioned 145 cm behind the examined sample. The experiments were performed in a vacuum chamber at a controlled temperature of 90 °C.

The diffractograms were recorded over a period of 5 h (45 kV on the tube and a current of 0.9 mA). The scattering intensity was recorded at intervals in the range of $0.07 < q < 2.8$ nm$^{-1}$. The wave vector was defined as $q = (4\pi/\lambda)\sin(\theta)$, where $2\theta$ is the scattering angle and $\lambda$ is the radiation wavelength (0.1542 nm). The scattering of capillary, solvent, and device electron noises were subtracted from the SAXS record.

## 3. Results and Discussion

The goal of this work was to analyze and establish the effect of polymer organization in solution and the connectivity between the two blocks in case of a BCP on the kinetics of NP formation. We have studied the kinetic behavior of all three metal systems using infrared spectroscopy. However, because all of the phenomena observed via our kinetic measurements seemed to be "universal" and apply to all metal carbonyl precursors that were examined, we have concentrated additional analyses mostly to the iron oxide and chromium oxide nanoparticle systems.

To eliminate the effect of solution viscosity, known to have a dramatic effect on reaction kinetics,[32] all reactions were conducted with a constant polymer concentration. Because of the weak interactions of PS with the metal surface, its presence in the solution and its function as a stabilizer has little effect on the kinetics.

Figure 1 shows the plots of the decomposition reactions of $Cr(CO)_6$ in two solutions: one containing PS and one without any stabilizer (i.e., PS). The superposition of the two curves indicates that the decomposition reactions in pure solvent and in a PS solution follow the same kinetics, further supporting the claim that the low polymer concentration does not increase solution viscosity enough to affect reaction kinetics.

A general reaction scheme,[21,31] typical for the decomposition of metal carbonyl complexes in solution to form metal oxides, is shown in Figure 2. Reaction mechanism suggests the formation of highly reactive intermediate metal carbonyl species, which do not accumulate during the reaction, resulting in the formation of stable metal oxide nanoparticles.

The thermolysis of chromium hexacabonyl ($Cr(CO)_6$) was monitored by following the intensity of one of its typical absorbance bands, specifically the one at 1977 cm$^{-1}$, which corresponds to the symmetric carbonyl stretching vibration, as shown in Figure 3. Similar spectroscopic data were collected

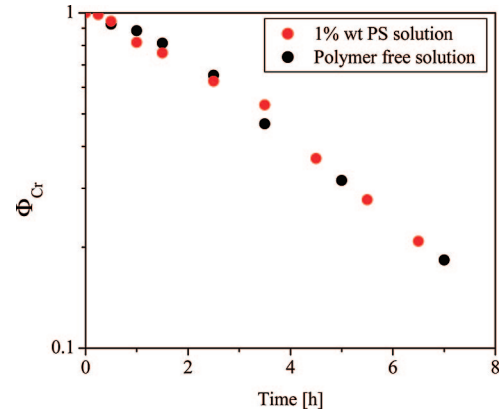


**Figure 1.** Decomposition reaction kinetics of chromium hexacarbonyl ($Cr(CO)_6$) in solution without polymeric stabilizers and in the presence of PS.

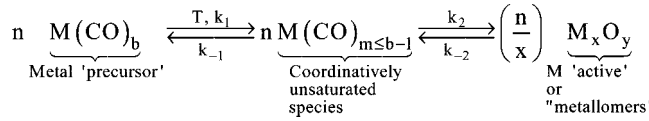


**Figure 2.** General reaction scheme for the decomposition of metal carbonyl precursors via the thermolysis reaction.

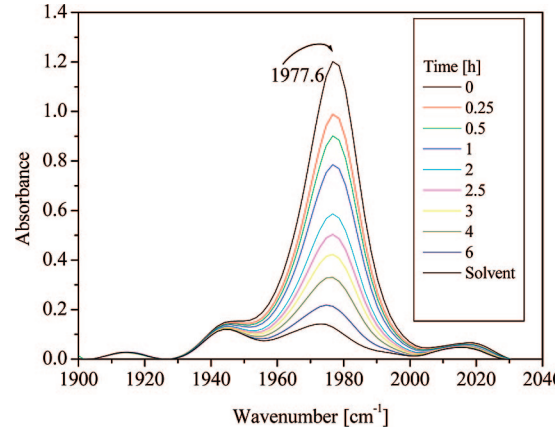


**Figure 3.** Fourier-transform infrared spectra of the $Cr(CO)_6$ absorption band at 1977 cm$^{-1}$, corresponding to the symmetric carbonyl stretching vibration.

for the decomposition reactions of iron pentacarbonyl ($Fe(CO)_5$) and dicobalt octacarbonyl ($Co_2(CO)_8$), having the corresponding analytical carbonyl stretching vibrations at 1996 and 2019 cm$^{-1}$, respectively. No infrared absorption bands associated with the formation of intermediates during the reaction can be observed in any of the different systems, suggesting that these intermediates do not accumulate. Hence, the mass balance on the metal atoms indicates that the number of metal atoms in the clusters is equal to the initial metal concentration in the precursor minus the unreacted precursor, and thus $\partial\phi_{cluster}/\partial t \approx -\partial\phi_{precursor}/\partial t$, where $\phi$ is the concentration of the species and $t$ is the reaction time.[33] This implies that the kinetic of the precursor decomposition describes, to a good approximation, the kinetic of particle formation.

Figure 4 shows the decomposition curves normalized to the initial concentration for the reaction of $Fe(CO)_5$. As can be seen, all curves follow an exponentially decaying function, corresponding to a first-order kinetics, which is typical of metal carbonyl decomposition reactions in solution.[33] By comparing the effect of the type of polymer present in solution, it is apparent that the reaction rate measured in the PMMA solution

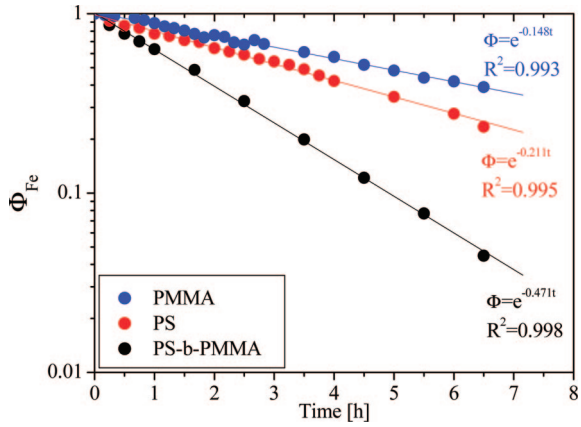


**Figure 4.** Decomposition kinetics of iron pentacarbonyl precursor in polymeric solutions plotted on a semilog scale of the normalized concentration as a function of time.

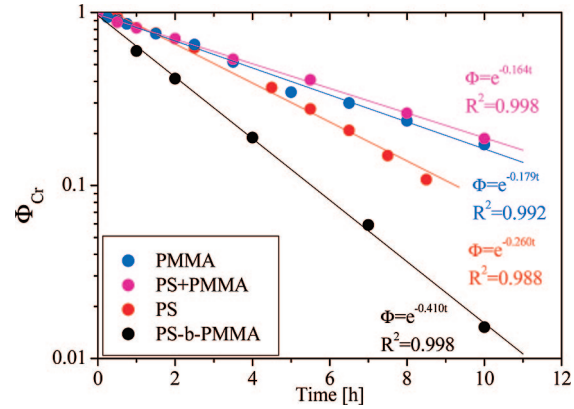


**Figure 5.** Decomposition kinetics of chromium hexacarbonyl precursor in polymeric solutions plotted on a semilog scale of the normalized concentration as a function of time.

is the lowest, with a rate constant of $k_d = 0.148\ h^{-1}$, in the PS solution it is faster, with a $k_d = 0.211\ h^{-1}$, while in the BCP solution the reaction is the fastest, with a $k_d = 0.471\ h^{-1}$. The same kinetic features are observed also when conducting the decomposition reaction with $Cr(CO)_6$ and $Fe(CO)_5$ as the precursors, as seen in Figure 5. The differences in the kinetic characteristics between the PS and PMMA solutions may be explained by taking into account the type of interactions that occur between the polymer and the metal species in the reaction medium. PS forms relatively weak dipole−dipole interactions with the metal species, while PMMA forms coordinative bonds that constitute much stronger interactions. However, the strong coordinative bond formed by PMMA with the metal surface has also the effect of lowering the reaction rate as compared to that observed with the PS. Furthermore, from Figure 5 it can be seen that by conducting the reaction in solutions containing a mixture of the homopolymers of PS and PMMA, the kinetic trend aligns with the one set by the PMMA. Performing the same reactions with $Co_2(CO)_8$ as the precursor reveals the same kinetic behavior as observed for the other two metals. These results clearly show that when PMMA is present in the solution it has a dominant effect on reaction kinetics due to its much more extensive interactions with the metallic species.

When the polymer in solution is the PS-*b*-PMMA BCP, the presence of the PMMA segment should have influenced the reaction rate such that it should have conformed to the trend set by the competitive chemical nature of both PMMA and PS; that is, it should have been dominated by the presence of PMMA

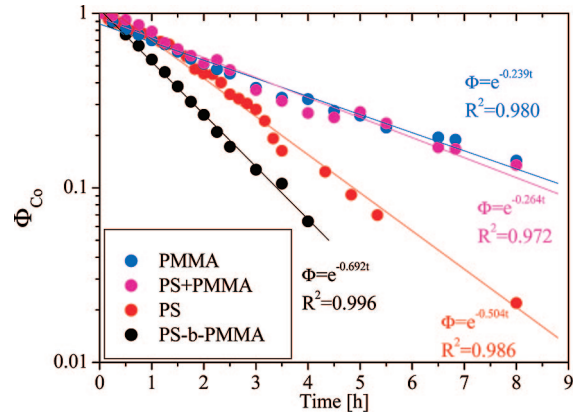


**Figure 6.** Decomposition kinetics of dicobalt octacarbonyl precursor in polymeric solutions plotted on a semilog scale of the normalized concentration as a function of time.

and hence been slower than the observed rate in either PS or mixed homopolymer media. However, as can be seen from Figures 4−6, the reaction rate in the BCP solution is about 3 times faster than that observed in the PMMA solution. Furthermore, from the data seen in Figures 1 and 5, it is also evident that the rate of reaction in the presence of BCP is much faster than the one observed in the absence of polymer, that is, conducted in the respective pure solvent alone!

Comparing TEM data with the kinetic behavior measured during the reaction can aid in understanding the NPs thermodynamic equilibrium size and size distribution. Figure 7 shows TEM micrographs of chromium oxide NPs formed in the various polymeric media. Figure 7a shows large NPs formed in the presence of PS. The stabilization of the NPs by the polymer occurs via the anchoring of the polymer segments onto the surface of the metal NP, resulting in the capping of the NPs by the polymer chains.[21,28] Furthermore, the adsorption of the polymer reduces the effective surface energy of the growing metallic fragments, thereby preventing their flocculation.[30,33] However, the weak dipole−dipole interactions of PS with the metal result in a poor surface stabilization and consequently are responsible for the formation of large ($d \approx 70$ nm) particles.[33] The dynamic nature of the interactions in the solution combined with the weak metal−polymer bond affords the highly reactive, unsaturated metal carbonyl species an opportunity to interact with other reactive metal fragments rather than with the polymer. In this case, the loss of conformational entropy by the polymer chain upon interaction with the metallic fragment is larger than the energy gained by creating an interface with the metal surface. Therefore, the NPs continue to interact with other metallic moieties until they reach a certain equilibrium size that is determined by their mobility in the medium and by the strength of the polymer−metal interactions. In contrast, Figure 7b shows small ($d \approx 2$ nm) NPs formed in the presence of PMMA. As was mentioned previously, PMMA forms strong coordination bonds with the highly reactive surface of the metal−oxide fragments. The interaction of PMMA with the metal lowers the free energy of the NPs and thereby reduces the tendency to interact with other highly reactive metal species present in the solution. PMMA also functions as a steric hindrance agent with respect to the van der Waals interactions between metallic fragments. Figure 7c shows chromium NPs formed in a PS-*b*-PMMA solution. It can be seen that the particles are similar in size ($d \approx 2$ nm) and shape to the ones formed in solutions containing PMMA alone. This suggests that the same mechanism controlling the morphology of the NPs in

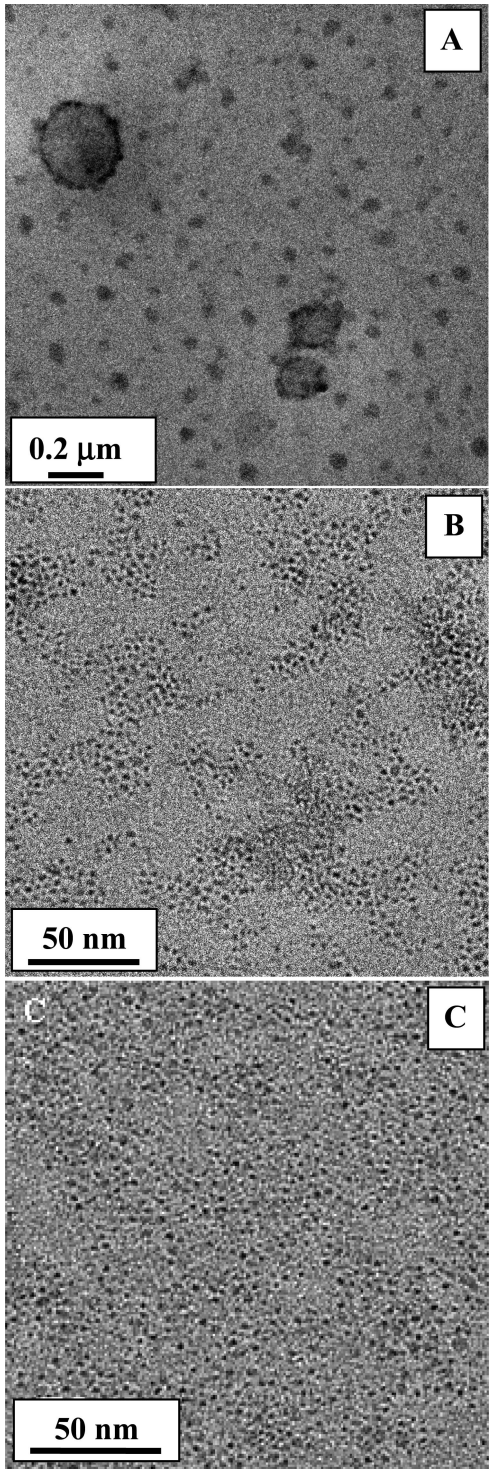


**Figure 7.** TEM micrographs of $Cr_2O_3$ nanoparticles in polymeric matrices after solvent evaporation: (A) PS, (B) PMMA, (C) PS-*b*-PMMA.

the PMMA solution can also account for that of the NPs formed in a BCP solution. The smaller particle size as compared to those formed in PS is the result of a nucleation-controlled reaction where the formation of many highly reactive nucleation sites is driven by the presence of PMMA, and where the capping of the nanoparticles by the polymer occurs through the formation of strong coordination bonds between the PMMA ester group and the NP surface.[21,33−36] Hence, the correlation of particle morphology to the dominant features of the polymeric medium in which they were created (i.e., nucleation-dominated in the presence of PMMA and growth-dominated in the presence of PS) cannot account for the reaction kinetics observed in the BCP medium. Therefore, the reason for the different kinetic behavior in the presence of the BCP must have a different origin.

Metal carbonyl complexes undergo a disproportionation reaction in solvents with Lewis base characteristics, such as dimethylformamide (DMF), 2-ethoxy ethanol, and tetrahydrofuran (THF), which are "good solvents" for PMMA.[37] To avoid this disproportionation, all reactions were conducted in a solvent that is considered either a "good solvent" for PS or nonpreferential for both polymers. Therefore, we expected that the BCP in this solvent will exhibit some degree of morphological arrangement, depending on the extent of the selective polymer−solvent affinity. Much experimental and theoretical work has been done regarding the arrangement of BCP chains in solutions where the solvent acts as a "good solvent" for one block and "bad solvent" for the other. For example, Noolandi et al.[36] used equilibrium statistical mechanics to calculate the size of the insoluble core, the outer shell, and the number of molecules per micelle formed in such a selective solvent, and their results were in good agreement with SAXS data obtained for the same system.[38] Evers et al. used statistical thermodynamics to study the adsorption of BCP polymer micelles on surfaces from asymmetric solvents, which enabled the calculation of the dimensions of the micelles and the critical micelle concentration (CMC).[25] Kotaka et al. used dynamic light scattering (DLS) to investigate the morphology of PS-*b*-PMMA in a mixture of solvents.[26] It is important to note that, in our particular case, the solvents used in the reactions do not behave as good and bad solvents for both PS and PMMA. Moreover, cyclohexanone is generally accepted as a nonpreferential solvent, and toluene is considered to solvate both PS and PMMA while being a better solvent for PS.

To exhibit the same thermodynamic behavior in the same solvent, two polymers would have to possess the same $\chi$ parameter (the Flory parameter), which is highly unlikely, especially for chemically different polymers, such as PS and PMMA.[37] However, because the homopolymers of both PS and PMMA do indeed dissolve in the solvents used under reaction conditions, the corresponding pure BCP should not necessarily self-assemble into a micellar morphology solely based on the individual block affinities toward the solvent. We propose that the formation of a micellar structure under these circumstances is the result of the selective interactions and a synergistic effect between the BCP and the metallic precursors in the reaction solution, which translate into an asymmetry regarding the affinity of each block toward the solvent. During the reaction, the metallic precursors interact primarily with the PMMA block, generating a self-assembled, core−shell structure in which the metallic precursor together with the PMMA block reside on the inside of the structure, surrounded by a PS shell, as seen in Figure 8A. This arrangement generated a high local precursor concentration inside the PMMA domain, resulting in an accelerated reaction rate (according to the first-order expression: $R_d = -d[\text{precursor}]/dt = k_d[\text{precursor}]$), and essentially transforming these domains into nanoreactors.[17,39] It is also possible that the close physical proximity between the ester group of the PMMA block and the decomposing metal precursor contributed to the amplified reaction rate by lowering the energy needed to extract a CO ligand from the coordination sphere of the metallic complex (according to the expression: $k_d = A_d \exp(-E_d/RT)$, which indicates that lowering the activation energy results in a higher reaction rate constant). However, the occurrence of such a morphological arrangement has not yet

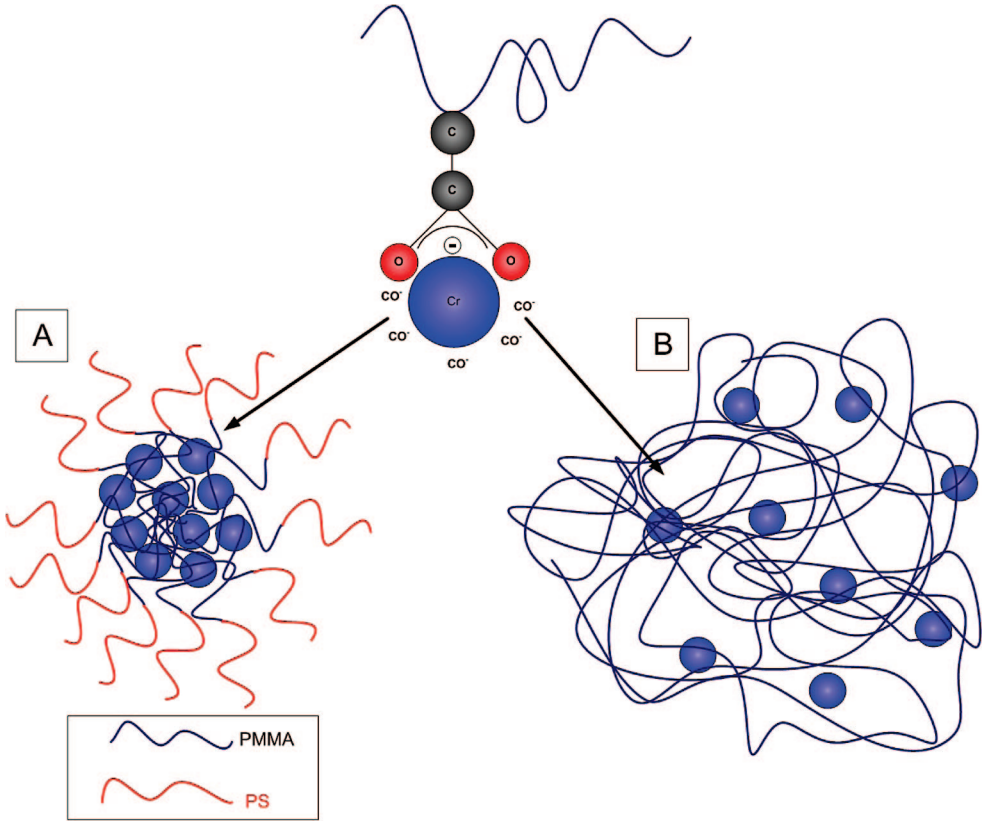


**Figure 8.** Schematic representation of the process responsible for metal oxide nanoparticle formation and interaction, demonstrating the difference between PMMA and BCP solutions.

been determined experimentally. The schematic representation in Figure 8B describes the behavior of the reaction performed in a solution composed of only PMMA dissolved in a relatively nonfavorable solvent, such as toluene. In this case, the dimensions of the PMMA chains (gyration radius, $R_g$) will be set by the energy of interaction with the solvent and the entropic energy of the free coils. As no micellar-like domains were formed, the precursor concentration in the PMMA solution is the actual bulk concentration, and, therefore, the reaction rate is determined by the customary thermodynamic conditions such as temperature, concentration, viscosity, and the strength of interaction between the growing metallic fragments with the polymer.

To examine the behavior of the BCP in the solution, we performed small-angle X-ray scattering (SAXS) measurements on the BCP solution at the actual temperature at which the reaction was conducted. Figure 9 shows the logarithmic plot of the normalized intensity as a function of the scattering vector $q$ for a 1 wt % BCP solution. In dilute polymer solutions, a negligible slope at small $q$ values suggests the presence of a globular morphology, such as that found in a micellar system.[40] However, our data do not fit the micellar model. Because the scattering intensity for particles in solution is proportional to the difference in electron density $(\rho_2 - \rho_1)^2$, PS in cyclohexanone does not show any scattering pattern in the SAXS experiments (data are not presented here). Therefore, the scattering from the PS-*b*-PMMA solution is clearly related to the PMMA chains. The best fit is obtained using Debye's Gaussian model,[40] describing a polymer coil in solution, and suggesting a radius of gyration ($R_g$) of 4.35 nm. Because the characterization using SAXS experiments relies on model fitting, it cannot be used as a stand-alone method, but requires supporting experimental evidence, in this case, from cryo-TEM experiments. Using cryo-TEM affords examination of vitrified

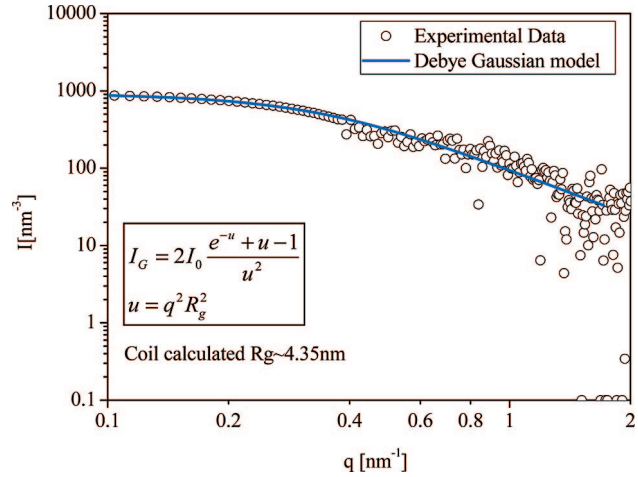


**Figure 9.** SAXS measurements of BCP in solution showing the plot of the intensity as a function of the scattering vector $q$ on a log−log scale. The data presented here are in absolute units and were normalized according to the capillary thickness, time, initial intensity, and transmittance value.[40]

specimens while in the solution state. The technique has been used to image micelles formed by several types of block copolymer. An ordered structure, such as a micelle, creates phase contrast between the polymeric domain and the surrounding solvent, while a polymer coil in solution does not give sufficient contrast for imaging.[41] Neither SAXS nor cryo-TEM data of the pure BCP solution indicated the formation of domains having specific morphology.

While these results pertain to BCP solutions in the absence of organometallic precursor, it is possible that the combination of BCP and metallic precursors in solution encourages phase segregation to a micellar morphology, thus changing the

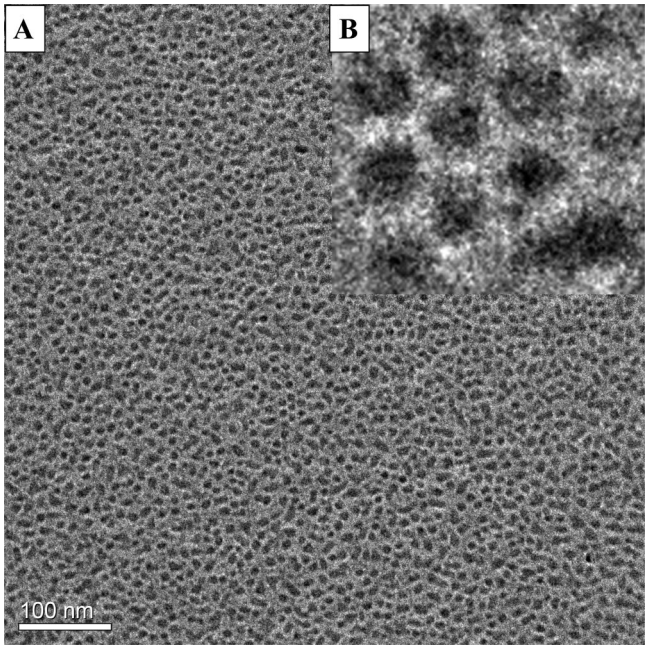


**Figure 10.** Cryo-TEM image of a toluene solution of BCP with $Fe(CO)_5$ precursor. The solution was heated to 60 °C for a few minutes to obtain thermal equilibrium before vitrified in liquid $N_2$. (A) Image shows ~7 nm BCP micelles in solution. (B) Digitally magnified section of image (A); the presence of metallic precursor in the core of the micelles produces the strong contrast observed in the image.

properties of the BCP in solution. By vitrifying a specimen of an extracted sample containing both BCP and precursor at the beginning of the reaction, it should be possible to examine reaction condition and determine the behavior of the composite solution. Unfortunately, it is not possible to fixate (vitrify) the solution of BCP with the unreacted precursor at the desired temperature for SAXS analysis, because the exposure of the precursor to the reaction temperature will immediately trigger the onset of reaction. To prepare a sample for cryo-TEM that will truly reflect the initial dispersion of the organometallic precursor in the polymer solution, the BCP solution had to be heated first to the reaction temperature and only then combined with the precursor. The sample was stirred briefly (for 1 min, to avoid temperature fluctuations) before it was quenched in liquid $N_2$. Figure 10A shows a cryo-TEM image of BCP micelles ($d \approx 7$ nm) containing $Fe(CO)_5$ precursor in toluene. Figure 10B shows a section of Figure 10A, digitally enlarged, revealing the accumulation of the metallic precursor inside the micelle core. The same method was also implemented on BCP containing $Cr(CO)_6$ precursor micelles ($d \approx 7$ nm) in a cyclohexanone solution (image not included).

Thus far, we have shown that the decomposition reaction in the presence of the BCP is consistently faster than that observed in all of the other solutions containing various combinations of PS and PMMA hompolymers. We also showed that a BCP solution in cyclohexanone or toluene containing an organometallic precursor, at the reaction temperature of 90 °C, does in fact form a dense morphology of PMMA (core) with a surrounding shell of PS. To relate the kinetic findings to this attributed morphology, we repeated our reactions in solutions containing asymmetric BCP, that is, BCP in which the two blocks differed in their lengths (i.e., molecular weights). Figure 11 shows a comparison between the reaction rates in a symmetric BCP and the rates in an asymmetric BCP. Figure 11a clearly shows that the increase of the molecular weight of the PMMA block with respect to the PS block to generate a

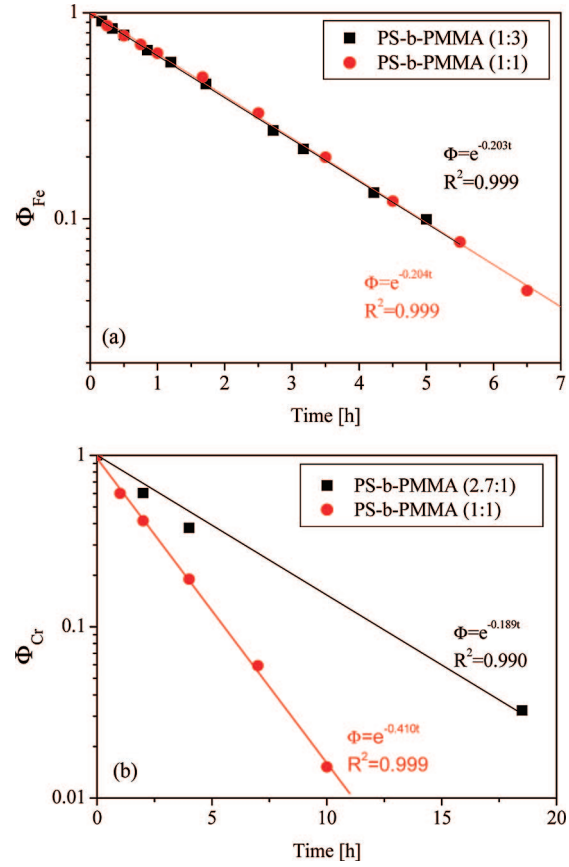


**Figure 11.** Semilog plot of the normalized concentration of (a) iron pentacarbonyl and (b) chromium hexacarbonyl as a function of time. The plots show a comparison of the reaction kinetics performed in an asymmetric BCP solution with one done in a symmetric BCP solution.

block ratio of 3:1, respectively, does not affect the reaction rate as compared to the reaction conducted in the symmetric BCP (1:1 block ratio, see Figure 4). However, Figure 11b shows that the increase in the molecular weight of the PS block with respect to the PMMA block to generate a block ratio of 2.7:1, respectively, causes the measured decomposition rate to follow the trend set by the PMMA alone (see Figure 5 for the PMMA curve). In this latter case, the larger fraction of the PS block, which is more soluble then PMMA in both cyclohexanone and toluene, caused an increase in the solubility of the BCP and resulted in a morphology commensurate with a free polymer coil in solution. Under these circumstances, the reaction rate is dominated by the strong coordinative bond between the metallic fragments and the PMMA block rather than by the constraints and effects of the condensed dimensions of the PMMA domains in a symmetric BCP or a BCP with a larger PMMA fraction.

We have stated earlier in this Article that our method for the preferential incorporation of metallic NPs into only one of the domains of a BCP can be used to produce a PBG material. Using the spin-coating method to evaporate the solvent, we can generate thin films consisting of the composite material that has both the scattering properties of the metallic NPs while maintaining the ability of the BCP to self-assemble into its thermodynamically preferred morphological order. Figure 12 shows a lamellar morphology of a symmetric BCP−NP composite film after a short period of annealing (4 h). Clearly, to achieve the characteristic properties required for a PBG material, the alignment of the lamellar structure must be perfected. However, as can be seen, the tendency of the

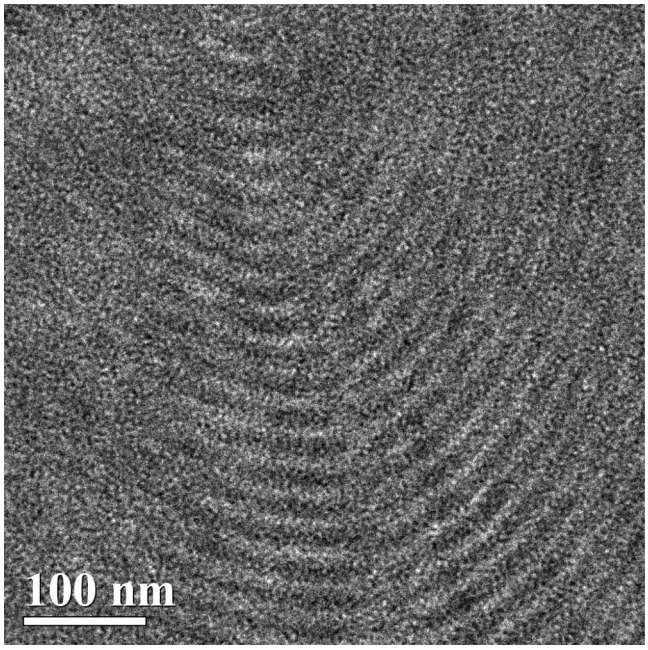


**Figure 12.** TEM micrograph of an unstained symmetric PS-*b*-PMMA BCP with $Cr_2O_3$ NPs showing lamellar morphology after a short annealing period of 4 h.

BCP−NP composite material to phase separate into the thermodynamically preferred morphology has not been compromised by the presence of the NPs in a preferred domain. The details and the optimization of the preferential segregation of NPs into a particular BCP domain are addressed separately.[42]

## 4. Conclusions

In this work, we have shown that the one-pot, in situ synthesis of metal nanoparticles from organometallic precursors in PS-*b*-PMMA BCP solutions is essentially catalyzed by the formation of condensed PMMA domains acting as nanoreactors, which gave rise to much faster reaction rates. On the basis of this faster reaction kinetics, we were able to show experimentally for the first time that the segregation of the metallic species in the PMMA domain occurs already in the initial stages of solutions preparation, and not in the later stages of the nucleation and growth processes. Moreover, we also showed that the assembly of the BCP in nonpreferential solvents into micellar domains did not occur with the pure BCP, but rather was promoted once the organometallic precursor was introduced into the BCP solution. Hence, the synergistic coupling between the metal carbonyl precursor and the BCP was the determining factor in the formation of the domain morphology of the BCP in solution. Interestingly, the metal oxide nanoparticles formed by this thermolysis reaction in BCP solutions were similar in shape and size to those generated in pure PMMA solutions. This indicates that the particle morphology is determined not by the kinetic of their formation but by their interactions with their surrounding media and the presence of reactive stabilizing molecules, such that, in this case, PMMA segments, either as homopolymers or as part of a BCP.

**Acknowledgment.** This research was supported by the Israel Science Foundation, Grant No. 650/06, by the European Union Marie Curie International Reintegration Grant (IRG), No. 036577, and by The National Science Foundation, Award ID ECS-0535382. We are indebted to Ms. Yehudit Schmidt and Dr. Ellina Kesselman from the Department of Chemical Engineering at the Technion for their expertise and assistance with the cryo-TEM imaging.

## References and Notes

(1) Yoon, J.; Lee, W.; Thomas, E. L. *MRS Bull.* **2005**, 721–726.
(2) Scrimgeour, J.; Sharp, D. N.; Blanford, C. F.; Roche, O. M.; Denning, R. G.; Turberfield, A. J. *Adv. Mater.* **2006**, *18*, 1557–1560.
(3) Povey, I. M.; Whitehead, D.; Thomas, K.; Pemble, M. E.; Bardosova, M. *Appl. Phys. Lett.* **2006**, *89*, 104103.
(4) Schartner, S.; Golka, S.; Pflugl, C.; Schrenk, W.; Strasser, G. *Microelectron. Eng.* **2006**, *83*, 1163–1166.
(5) Tadd, E. H.; Bradley, J.; Tannenbaum, R. *Langmuir* **2002**, *18*, 2378–2384.
(6) Bates, F. S.; Fredrickson, G. H. *Annu. Rev. Phys. Chem.* **1990**, *41*, 525–557.
(7) Hiemenz, P. C. *Polymer Chemistry−The Basic Concepts*; Marcel Dekker, Inc.: New York, 1984.
(8) Ohta, T.; Ito, A. *Phys. Rev. E* **1995**, *52*, 5250–5260.
(9) Bockstaller, M. R.; Mickiewicz, R. A.; Thomas, E. L. *Adv. Mater.* **2005**, *17*, 1331–1349.
(10) Fink, Y.; Urbas, A. M.; Bawendi, M. G.; Joannopoulos, J. D.; Thomas, E. L. *J. Lightwave Technol.* **1999**, *17*, 1963–1969.
(11) Fink, Y.; Winn, J. N.; Fan, S.; Chen, C.; Michel, J.; Joannopoulos, J. D.; Thomas, E. L. *Science* **1998**, *282*, 1679.
(12) Hamdoun, B.; Ausserr, D.; Joly, S.; Gallot, Y.; Cabuil, V.; Clinard, C. *J. Phys. II* **1996**, *6*, 493–501.
(13) Lin, Y.; Boker, A.; He, J.; Sill, K.; Xiang, H.; Abetz, C.; Li, X.; Wang, J.; Emrick, T.; Long, S.; Wang, Q.; Balazs, A.; Russell, T. P. *Nature* **2005**, *434*, 55–59.
(14) Urbas, A.; Fink, Y.; Thomas, E. L. *Macromolecules* **1999**, *32*, 4748–4750.
(15) Deshmukh, R. D.; Composto, R. J. *Chem. Mater.* **2007**, *19*, 745–754.
(16) Balazs, A. C. *Curr. Opin. Solid State Mater. Sci.* **2003**, *7*, 27–33.
(17) Wang, Q.; Nealey, P. F.; Pablob, J. J. D. *J. Chem. Phys.* **2003**, *118*, 11278–11285.
(18) Gosa, K. L.; Serban, S.; Christopoulou, V.; Papanagopoulos, D.; Dondos, A. *Polym. Plast. Technol. Eng.* **2000**, *39*, 95–104.
(19) Chiu, J. J.; Kim, B. J.; Kramer, E. J.; Pine, D. J. *J. Am. Chem. Soc.* **2005**, *127*, 5036.
(20) Zhang, Q.; Gupta, S.; Emrick, T.; Russell, T. P. *J. Am. Chem. Soc.* **2006**, *128*, 3898.
(21) King, S.; Hyunh, K.; Tannenbaum, R. *J. Phys. Chem. B* **2003**, *107*, 12097–12104.
(22) Tannenbaum, R.; Zubris, M.; Goldberg, E. P.; Reich, S.; Dan, N. *Macromolecules* **2005**, *38*, 4254–4259.
(23) Toshima, N.; Shiraishi, Y.; Teranishi, T. *J. Mol. Catal. A* **2001**, *177*, 139–147.
(24) Edwards, C. J. C.; Richards, R. W.; Stepto, R. F. T. *Polymer* **1986**, *27*, 643–650.
(25) Evers, O. A.; Scheutjens, J. M. H. M.; Fleer, G. J. *Macromolecules* **1990**, *23*, 5221–5223.
(26) Kotaka, T.; Tanaka, T.; Hattori, M.; Inagakilb, H. *Macromolecules* **1978**, *11*, 138.
(27) Kotaka, T.; Ohnuma, H.; Inagaki, H. *Polymer* **1969**, *10*, 517–529.
(28) Netz, R. R.; Andelman, D. *Phys. Rep.* **2003**, *380*, 1–95.
(29) Dan, N. *Langmuir* **2000**, *16*, 4045–4048.
(30) Tadd, E.; Zeno, A.; Zubris, M.; Dan, N.; Tannenbaum, R. *Macromolecules* **2003**, *36*, 6497–6502.
(31) Tannenbaum, R.; King, S.; Lecy, J.; Tirrell, M.; Potts, L. *Langmuir* **2004**, *20*, 4507–4514.
(32) Tannenbaum, R. *Inorg. Chim. Acta* **1994**, *227*, 233–240.
(33) Dan, N.; Zubris, M.; Tannenbaum, R. *Macromolecules* **2005**, *38*, 9243–9250.
(34) Ozkar, S.; Finke, R. G. *J. Am. Chem. Soc.* **2002**, *124*, 5706.
(35) Watzky, M. A.; Finke, R. G. *J. Am. Chem. Soc.* **1997**, *119*, 10382.
(36) Tannenbaum, R.; Hakanson, C.; Zeno, A.; Tirrell, M. *Langmuir* **2002**, *18*, 5592–5599.
(37) Miller-Chou, B. A.; Koenig, J. L. *Macromolecules* **2003**, *36*, 4851–4861.
(38) Noolandi, J.; Hong, K. M. *Macromolecules* **1983**, *16*, 1443–1448.
(39) Joly, S.; Kane, R.; Radzilowski, L.; Wang, T.; Wu, A.; Cohen, R. E.; Thomas, E. L.; Rubner, M. F. *Langmuir* **2000**, *16*, 1354–1359.
(40) Glatter, O.; Kratky, O. *Small Angle X-ray Scattering*; Academic Press, Inc.: London, 1982.
(41) Hamley, I. W.; Castelletto, V.; Fundin, J.; Yang, Z.; Crothers, M.; Attwood, D.; Talmon, Y. *Colloids Surf., A* **2004**, *282*, 514–517.
(42) Partially presented at the Fall ACS National Meeting. Gazit, O.; Tannenbaum, R. Polymer Preprints. National Meeting of the American Chemical Society, Boston, MA, 2007; 48, 615–616.

JP807668H